Proceedings of the 17th Pan-American Conference on Soil Mechanics and Geotechnical Engineering (XVII PCSMGE), and 2nd Latin-American Regional Conference of the International Association for Engineering Geology and the Environment (IAEG), La Serena Chile, 2024.

Earth observation for landslides monitoring. The study case in Colombia.

Nixon A. Correa-Muñoz
Universidad del Cauca, Full profesor, Colombia, nico@unicauca.edu.co

Carol A. Murillo-Feo
Universidad Nacional de Colombia, Full profesor, Colombia

ABSTRACT: Earth Observation (EO) data has increased global research on the topics of recognition, monitoring, and evaluation of the geohazards. EO data, thematic layers, and ground-based measurements provide the input data for designing prediction models and monitoring geohazards. A geo-hazard is a potential risk to the population, property, infrastructure, and the environment. This paper aims to present a case study where terrain variables derived from EO are used to generate models by machine learning techniques that allow us to understand the mechanisms of geohazard generation, adopt preventive actions, and reduce the affectations and damages over infrastructure and environment. The study uses radar remote sensing data from a time series collection of the Copernicus-Sentinel-1 mission to generate a dynamic land cover map where landslides are highlighted using the change detection techniques from SAR intensity analysis. Vertical displacements using the SBAS technique in the range between -20 cm/year and 20 cm/year were calculated in the study area. These results provide information about the activity of the terrain associated with subsidence or uplifting movements.

KEYWORDS: earth observation, geohazard, synthetic aperture radar, change detection, displacement map.

1 INTRODUCTION.

Earth observation (EO) from space collects information on Earth's surface using remote sensing techniques with different sensors e.g. radar (radio detection and ranging). Radar remote sensing has the potential to detect and monitor geohazards across the analysis of the amplitude and phase difference of the signal due to it enabling observations day or night in all weather conditions from space.

Geohazards are events related to geological activity that could affect people, infrastructure, or the environment. One of the geological hazards is landslides, which are triggered by mechanisms such as earthquakes or rainfall. Landslides are the movement of a mass of rock, debris, or earth down a slope. The change detection technique can identify landslide locations (Tomás & Li, 2017).

The change detection technique simultaneously analyses two SAR images acquired from the same area. Unsupervised methods allow for extracting the changes; one of them is based on the generation of an image difference, and the other is the analysis of the difference images with methods to identify what pixels suffered a change or not (Gong et al., 2014).

Satellite radar interferometry is widely used in the research field to measure ground movements. Multi-interferograms SAR interferometry techniques allow the study of slow-moving landslides (velocity less than 1,6 m per year) according to (Cruden & Varnes, 1996). These techniques are Persistent Scatterers, PS-InSAR (Ferretti et al., 2001), and Small Baseline Subset (SBAS) (Berardino et al., 2002).

PS-InSAR compares SAR images collected at different times and with different baselines to provide terrain deformation with millimetric accuracy. One of the main limitations of this technique is that atmospheric inhomogeneity generates an atmospheric phase screen (APS) on each SAR image, affecting the accuracy of deformation monitoring. APS cannot be estimated from the coherence generated during the interferogram generation. But if coherent pixels over long time intervals (permanent scatterers) can be identified, then the InSAR dataset is exploited for the modelling of the local velocity field in the area under study (Ferretti et al., 2001).

SBAS technique is based on the appropriate combination of differential interferograms by data pairs acquired by small orbital separation (baseline) to reduce spatial decorrelation and topography errors. This technique increases the temporal sampling rate by using all the acquisitions of the small baseline subsets and provides spatially dense deformation maps (Berardino et al., 2002).

This article aims to apply flow processing to detect changes in an SAR intensity dataset and estimate the terrain deformation in the multi-temporal analysis of the interferograms generated by the SBAS technique.

1.1 *Study area*

The study area corresponds to a section of six kilometers in the road sector of Fusagasugá – Silvania – Bosa (Bogotá) in the middle central region of Colombia. The WGS coordinates corners are bounded by W74,406°, N4,418°, and W74,373°, N 4,467°covering an area of 19,85 km^2, in hilly topography with heights which vary between 1518,16 masl, and 2329,18 masl.

Figure 1 shows the full radar scene embedded in the study area. The section analysis is defined by the Silvania–Subia road, which crosses the south-north direction between the central mountain range. The zone is watered by rivers in the north-to-south direction and has several streams crossing the national road. A special characteristic of the zone's geomorphology is landforms with the shape of plan-concave arcs towards the road.

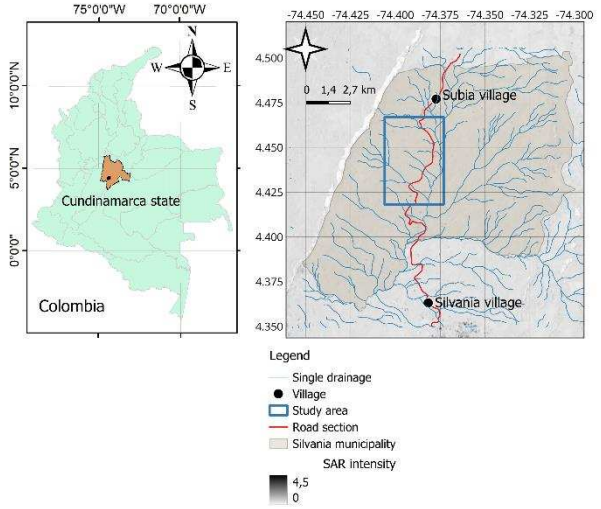

Figure 1. Study area in Cundinamarca state.

1.2 *Input data*

SAR scenes were downloaded from the European Space Agency (ESA) with the characteristics indicated in Table 1.

Table 1. Characteristics of the radar subset acquired by ESA's Copernicus.

Satellite/Series	*Sentinel-1*	*A/B*
Band/Polarization	C	VV/VH
Analysis period	2014	2022
GSD(m), swath (km)/revisit (days)	(5x20), 250	24

Fuentes: ASF Data Search Vertex: (https://search.asf.alaska.edu)

SAR scenes from ESA's Copernicus from October 2014 until November 2022 had VV polarization (314 images) and VH (251 images). The stack's orbital pass was ascending (226 images) and descending (339 images).

2. METHODOLOGY

The monitoring study was conducted in three phases: a) unsupervised classification of the study area with temporal statistics from time series of the radar backscattering, b) change detection based on cumulation sum and change magnitude and thresholds over differences of images, and c) estimation of the terrain deformation by SBAS InSAR technique.

2.1. Supervised classification

A stack of GRD Sentinel-1 images was built with the Graph Builder of the ESA's SNAP Toolbox. The flow processing applied the operations of thermal noise removal, applying orbit file, radiometric calibration, terrain correction, linear-to-from-dB, and subset. The product obtained via batch processing of all radar stack images was radiometrically calibrated, corrected by terrain distortions with a global digital elevation model, and amplitude values transformed into decibels (sigma0) and cutting on the study area with map coordinates (WGS84). The flow processing implemented in this paper is documented in (Braun, 2021).

It was necessary to apply an adaptive filter (Boxcar) to smooth the random variations of the radar signal. To visualize a temporal series of radar scenes the SNAP's stack tool calculates a new band with the series statistics: minimum, average, maximum, and standard deviation.

Each pixel's temporal information along the stack allows aggregation of similar object features. The K-means unsupervised method was used as a classifier. This method guarantees that each class represents attributes and that pixels are similar within the same class yet different between two classes. These results were complemented with a random forest-supervised method (Breiman, 2001), which was used as a training dataset for a landslide inventory of the zone built using field geomorphology recognition.

2.2. Change detection method.

A stack of radiometric-terrain-corrected (RTC) SAR scenes was acquired on NASA-ASF-vertex for descending passes to keep the geometric differences between images as low as possible. Then, a time series with backscattering values was created. The average was derived from pixels of the time series to obtain the cumulative sum and the residual for each band (time). Metrics of cumulative sum maximum and minimum and change magnitude were calculated.

Change magnitude was masked with a priori-threshold to identify change candidates. The picking of change points involved the bootstrapping resampling technique. Next, confidence metrics are extracted, and a threshold of change points is defined to identify the most likely change thresholds for a change map candidate. Finally, a raster layer is generated with the band of the first date after a change is detected. This methodology was implemented in Notebooks available on ASF-OpenSARLab on the website: (https://opensciencelab.asf.alaska.edu/).

2.3. Terrain deformation by SBAS InSAR technique.

This chain processing started with searching and generating interferograms stacked with 24 days of baseline in NASA's ASF-vertex. Interferograms correspond to flight orbital path 69 and descending orbital pass. Interferograms were acquired with the small baseline technique. A subset of rectangular shapes was created to reduce the swath to the study area. SmallBaseline.App.py was used to invert an unwrapped interferogram stack and apply corrections to obtain terrain displacement time series.

The analysis of the SBAS time series included a) identification and exclusion of interferograms affected by phase unwrapping mistakes, b) creation of interferograms network with attributes like dates, temporal average coherence, and baseline separation, coherence matrix of all available pairs, c) selection of reference point or pixel with the highest spatial coherence of the series, d) inversion of the SBAS network, e) DEM errors correction to obtain the residual topography phase, f) calculation of the root-mean-square error of the residual phase to remove the large wave component (outliers values), g) referencing of the time series respect to a specific date of the stack, h) velocity rate estimation to long term. Theoretical and practical aspects of the SBAS InSAR technique are documented in (Yunjun et al., 2019).

Another stage of the flow processing was the error analysis, which established the inversion quality by calculating the spatial average coherence to pick reliable pixels after temporal series inversion. Besides, temporal coherence was obtained to guarantee the consistency of the temporal series with the interferogram network. Estimated velocity and uncertainty expression are based on goodness of fit according to a linear model.

Finally, the results are displayed in maps, such as displacement for different periods and maps of the coherence, velocity, and total displacement in Geo Tiff format.

3 RESULTS

This section shows the main findings of the activities presented in the methodology with respective discussion.

3.1. Supervised classification

Figure 2 shows the temporal signature of a pixel-like example of the GRD-SAR intensity time series. This tool, available on ESA's SNAP Toolbox, allows visualizing the temporal variation of the SAR intensity expressed in decibel units. The variable displayed is Sigma0_VV_avg, which means that the time series corresponds to the average intensity of the analysis period in a specific pixel. The time series exposes temporal gaps highlighted in red due to the sensor not capturing information during revisit time.

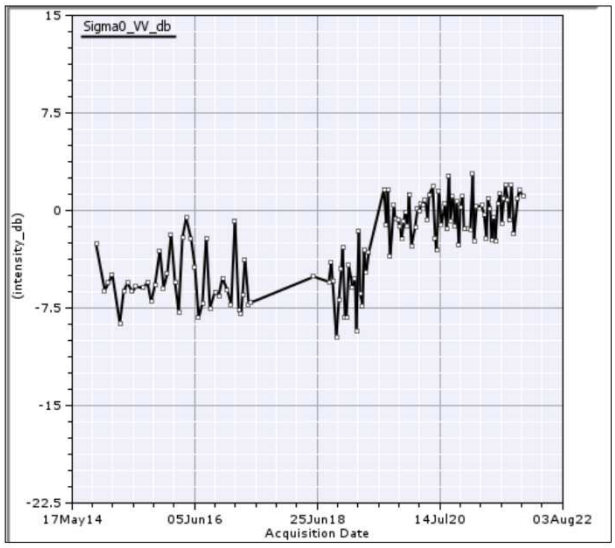

Figure 2. Temporal signature of a specific GRD-Sentinel-1 pixel of the study area, VV polarization.

Figure 3 shows the landslide inventory obtained by fieldwork overlapped on the time series stack of the temporal statistics of the GRD SAR intensity. The fieldwork was done at the end of the 2022 year by a commission of geologists and geotechnics of the IGL enterprise. Landslide inventory serves as training data for the supervised classification of the model.

Random Forest is one of the better methods to classify objects from the point of view of accuracy (Stumpf & Kerle, 2011). This classifier extracts all the pixels of the training polygons (landslides) and finds thresholds to separate the input data type. Figure 4 shows the landslide classification with radar backscattering variables and dual polarization in all the study areas. Polygons with the same colour as the classification but with black borders correspond to the landslide inventory. Accuracy classification was 73,4% for slow earth flow, 78,1 % for slides, and 84,2% for rapid detritus flow. This accuracy is explained in that the inventory done only described the mass movement affectations and not all the landscape land cover. Furthermore, the classification accuracy is in the same order found in (Taalab et al., 2018). The study area found similar zones from the point of view of radar backscattering in 47% of pixels for slow earth flow, 31,3% for slides, and 20,5% for rapid detritus flow.

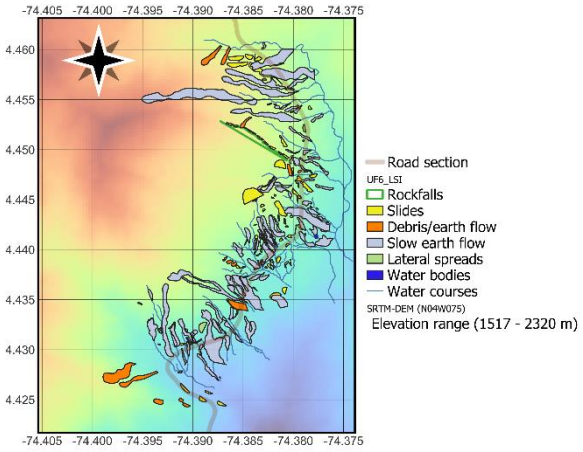

Figure 3. Mass movement classes in the study area.

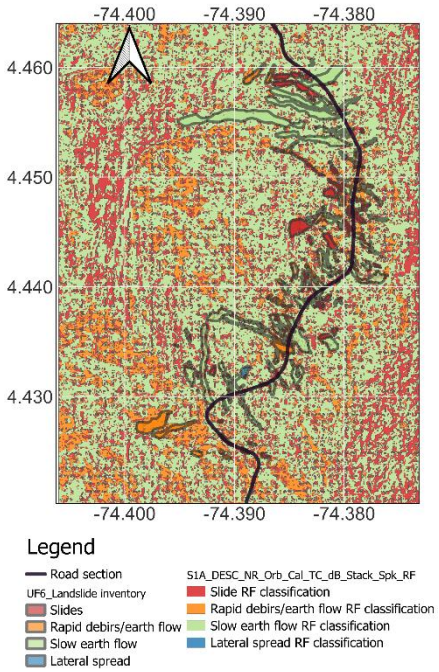

Figure 4. Random forest classification of landslides (GRD-Sentinel 1, descending).

3.2. Change detection method.

Figure 5 shows the maximum and minimum cumulative sum metrics, as well as the magnitude change of the stack demand with the characteristics of gamma radiometry, amplitude scale, 30 m pixel spacing, Copernicus DEM, and RTC L1 Detected High-Res Dual-Pol (GRD-HD) products. Magnitude change is calculated as the maximum and minimum cumulative sum difference. Most predominance of positive values indicated modifications associated with the growth of vegetation.

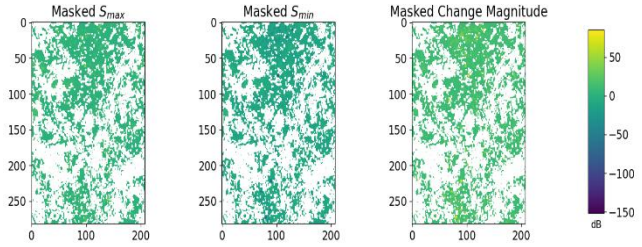

Figure 5. Cumulative sum metrics of the backscattering differences.

Change areas candidates are defined using thresholds analysing the cumulative distribution frequency of magnitude change, then by resampling the cumulative sum is recalculated over residuals of the time series to mask the change pixel candidates (see Figure 6).

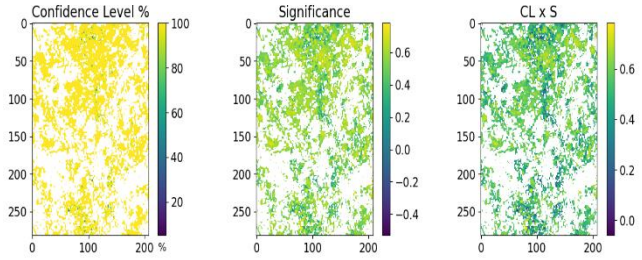

Figure 6. Cumulative sum metrics of the masked pixels.

Next, confidence metrics, such as confidence level, the significance of the change point, and the product of the values, are extracted as a confidence indicator to identify change points (see Figure 7).

Finally, the change pixels were detected using a change point threshold of 0,01. This threshold corresponds to a confidence level of 99%, indicating the most extreme changes. Another confidence level can be assumed to include other less critical changes. Figure 8 shows the change in pixels with the greater likelihood in the map of change candidates, dots in purpure color.

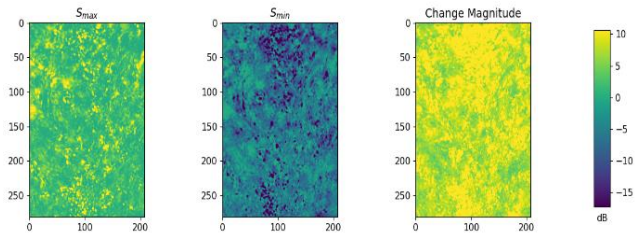

Figure 7. Confidence metrics for identification of change points.

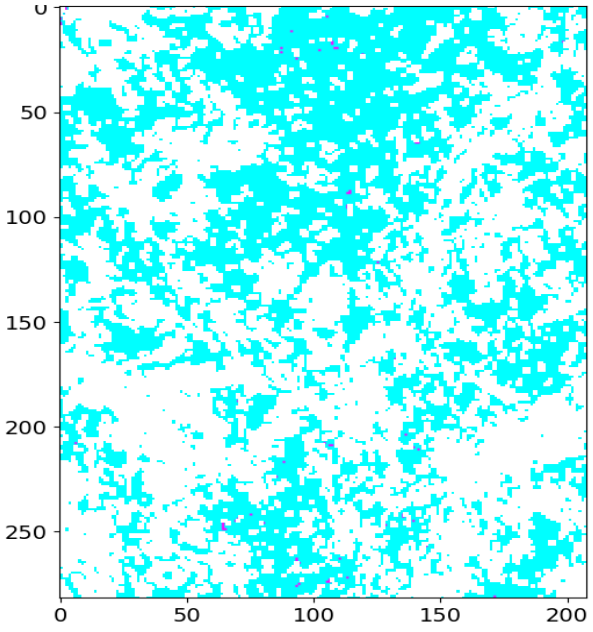

Figure 8. Change pixel detection using a threshold of 0.01.

On the other hand, also a threshold for the coefficient of variation can be set to classify change in the time series. So, the rule of thumb is t=CDF(CV) > 0.95 (5% pixels with the highest variance) producing the sites indicated in Figure 9.

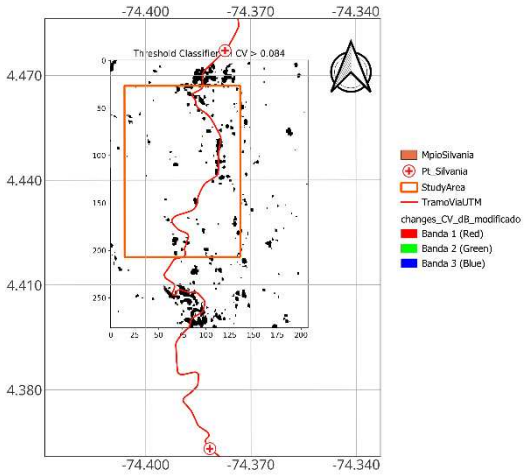

Figure 9. Change pixel detection using a CV threshold of 0,95

3.3. Terrain deformation by SBAS InSAR technique.

In this topic, the results found on October 31st, 2018, and December 14th, 2021, are presented. In the span indicated, 177 interferograms were obtained by demand from ASF-vertex in the flight path 69, descending pass orbit, and a reference point was automatically detected according to higher temporal coherence in the coordinates 74,38950°W and 4,33429°N. The maximum perpendicular baseline was 219 m, and coherence between 0,33 and 0,75 were

obtained (see Figure 10). Figure 10 shows the C-band dataset with temporal and spatial baseline. In particular, the SBAS interferogram network shows the average coherence in each interferogram, and the colour bar gives the values upper 0,2. More connections of SBAS interferograms are mainly vertical, meaning small temporal baselines are selected. Minimizing the distance reduces the topography, which could obscure the deformation. Minimizing the time between acquisitions avoids creating interferograms where terrain deformation is larger than the sensor wavelength (Ferretti et al., 2007).

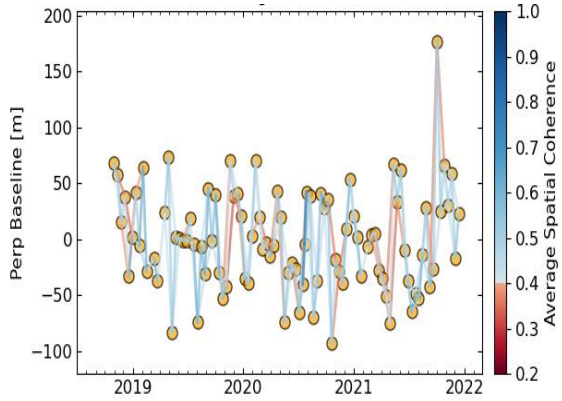

Figure 10. Geometric characteristics of the SBAS interferograms network.

Line-of-sight (LOS) InSAR velocity between -10,1 cm/year and 3,59 cm/year was estimated with a prediction error between 0,003 cm/year and 0,32 cm/year (see Figure 11). According to the velocity scale proposal (Cruden & Varnes, 1996), the detected range corresponds to the extremely slow and very slow landslide moving.

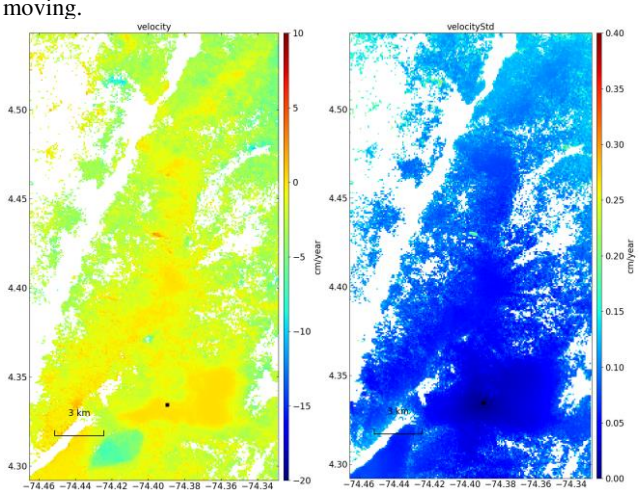

Figure 11. LOS-InSAR velocity and its error estimation.

The result is presented in Figure 12, where the variability of the displacements in the LOS direction overlaps with the Google Earth virtual globe. Ground deformation velocities are measured by the satellite in the direction of the line-of-sight (LOS), whereas real displacement occurs in three dimensions. This displacement is referred to the direction of the local maximum slope under the assumption that it is the most probable direction of real movement. Béjar-Pizarro et al. (2017) explains the formulas for calculating the velocity projected along the slope. The velocity slope range in the study area was between -12,9 cm/year and 4,6 cm/year. This range was more extensive than the LOS velocity since the minimum detected rate and the standard deviation were higher due to the significant dispersion of the SBAS InSAR pixels. LOS inventory in the lateral zones of the road is related to mean LOS velocity between—2 and 7 cm/year.

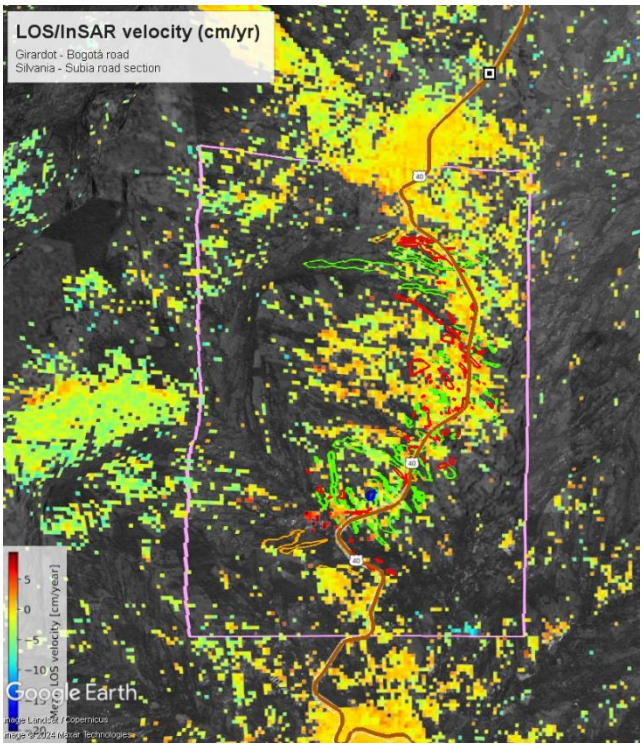

Figure 12. LOS-InSAR velocity on Google Earth.

4 CONCLUSIONS

Unsupervised classification, since training classes generated by geomorphology field work, allowed expanding the known classes (landslide inventory) at all study areas by searching for similar patterns of the multi-temporal SAR intensity signal.

The cumulative sum technique was applied over a stack of 153 GRD_HRD scenes of the Copernicus Sentinel-1 satellite, descending orbit, and VV polarization. This technique, combined with the iterative analysis of change pixels, allowed the definition of a magnitude change map, which was masked with thresholds to detect changes associated with a specific date. This information, combined with the fieldwork, should help with the interpretation of the motion of the study area.

The small baseline InSAR method estimated terrain deformation from October 2018 to December 2021. The range of LOS-InSAR velocity was between -10 cm/year and 3,6 cm/year, with error prediction less than 0,32 cm/year. The above respects a

reference point located in Fusagasugá town, which was automatically detected as the most stable point in the zone of study.

SAR intensity and SBAS-InSAR techniques are complementary analyses that provide information about the more critical changes in the terrain (change detection from SAR intensity) and the magnitude of deformation (LOS velocity) from SBAS-InSAR to determine the deformation pattern in the study area.

5 ACKNOWLEDGEMENTS

The authors are grateful to the enterprise Ingeniería y Geotecnia S.A.S., established in Bogotá (Colombia), for the financial support for conducting this multitemporal SAR study. We are also grateful to the NASA-Alaska Satellite Facility for online training and access to resources of ASF-OpenSARLab for implementing the SAR intensity and InSAR workflow algorithms available under the cloud computing approach.

6 REFERENCES

Béjar-Pizarro, M., Notti, D., Mateos, R. M., Ezquerro, P., Centolanza, G., Herrera, G., Bru, G., Sanabria, M., Solari, L., Duro, J., & Fernández, J. (2017). Mapping Vulnerable Urban Areas Affected by Slow-Moving Landslides Using Sentinel-1 InSAR Data. Remote Sensing, 9(9), 876. https://doi.org/10.3390/rs9090876

Berardino, P., Fornaro, G., Lanari, R., & Sansosti, E. (2002). A new algorithm for surface deformation monitoring based on small baseline differential SAR interferograms. IEEE Transactions on Geoscience and Remote Sensing, 40(11), 2375–2383. https://doi.org/10.1109/TGRS.2002.803792

Braun, A. (2021). Sentinel-1 Toolbox Time-series analysis with Sentinel-1. https://skywatch.co

Breiman, L. (2001). Random Forests. Machine Learning, 45(1), 5–32. https://doi.org/10.1023/A:1010933404324

Cruden, D., & Varnes, D. J. (1996). LANDSLIDE TYPES AND PROCESSES. In Landslide Types and Processes (Issue Transportation Research Board, U.S. National Academy of Sciences, Special Report, 247).

Ferretti, A., Monti-Guarnieri, A., Prati, C., & Rocca, F. (2007). InSAR processing: a practical approach. Part B.

Ferretti, A., Prati, C., & Rocca, F. (2001). Permanent scatterers in SAR interferometry. IEEE Transactions on Geoscience and Remote Sensing, 39(1), 8–20.

Gong, M., Li, Y., Jiao, L., Jia, M., & Su, L. (2014). SAR change detection based on intensity and texture changes. ISPRS Journal of Photogrammetry and Remote Sensing, 93, 123–135. https://doi.org/10.1016/j.isprsjprs.2014.04.010

Lanari, R., Casu, F., Manzo, M., Zeni, G., Berardino, P., Manunta, M., & Pepe, A. (2007). An overview of the Small BAseline Subset algorithm: A DInSAR technique for surface deformation analysis. Pure and Applied Geophysics, 164(4), 637–661. https://doi.org/10.1007/s00024-007-0192-9

Stumpf, A., & Kerle, N. (2011). Object-oriented mapping of landslides using Random Forests. Remote Sensing of Environment, 115(10), 2564–2577.

Taalab, K., Cheng, T., & Zhang, Y. (2018). Mapping landslide susceptibility and types using Random Forest. Big Earth Data, 2(2), 1–20. https://doi.org/10.1080/20964471.2018.1472392

Tomás, R., & Li, Z. (2017). Earth Observations for Geohazards: Present and Future Challenges. Remote Sensing, 9(3), 194. https://doi.org/10.3390/rs9030194

Yunjun, Z., Fattahi, H., & Amelung, F. (2019). Small baseline InSAR time series analysis: Unwrapping error correction and noise reduction. Computers & Geosciences, 133(104331), 1–95. https://github.com/insarlab/MintPy